14th International Symposium on Turbulence and Shear Flow Phenomena (TSFP14)
Heidelberg, Germany, July 28–31, 2026

TRANSITION BETWEEN LOCALISED AND SPACE-FILLING STATES OF PURELY ELASTIC TURBULENCE IN CHANNEL FLOWS

Damiano Capocci
School of Physics and Astronomy,
The University of Edinburgh
Peter Guthrie Tait Road
Edinburgh, EH9 3FD, UK
dcapocci@ed.ac.uk

Moritz Linkmann
School of Mathematics and
Maxwell Institute for Mathematical Sciences
The University of Edinburgh
Peter Guthrie Tait Road
Edinburgh, EH9 3FD, UK
Moritz.Linkmann@ed.ac.uk

Alexander Morozov
School of Physics and Astronomy,
The University of Edinburgh
Peter Guthrie Tait Road
Edinburgh, EH9 3FD, UK
Alexander.Morozov@ed.ac.uk

ABSTRACT

Viscoelastic fluids can exhibit chaotic flow states sustained purely by elastic stresses, commonly referred to as elastic turbulence, even when inertia is negligible. Recent studies (Lellep *et al.*, 2024; Morozov *et al.*, 2025) of purely elastic turbulence in pressure-driven channel flows have shown that, unlike Newtonian turbulence which is produced mainly near the walls, viscoelastic turbulence is organised around the channel centre-plane. In particular, the dynamics exhibit either a single isolated structure or space-filling states. Here, we examine the transition between these two regimes. A key feature is that space-filling states are characterised by lower kinetic energy than single-structure states. Extending the parameter space to more dilute and more elastic polymer solutions, we find that the spatio-temporal pattern is characterised by an isolated structure. We further compare polymeric stretching statistics, highlighting structural and statistical differences both between single-structure and space-filling dynamics within the same parameter regime and between single-structure states across different parameter regimes.

INTRODUCTION

Non-Newtonian fluids are ubiquitous in nature and applications, and can exhibit a wide range of flow behaviour, including colloidal shear-thickening, rod climbing in polymer solutions, and shear banding in worm-like micelles (Larson, 1999; Bird, 1987). Among these, dilute solutions of long, flexible polymer molecules constitute a class of complex fluids that display both fluid-like and solid-like behaviour. Under external forcing, such fluids can develop elastic turbulence, a chaotic flow state absent in Newtonian fluids such as water. In contrast to Newtonian turbulence, which is sustained by inertia, elastic turbulence is driven by the stretching of polymer molecules and can arise even when inertia is negligible.

Observations of elastic turbulence in experiments are well- documented in literature, starting from (Groisman & Steinberg, 2000), including curvilinear geometries (Groisman & Steinberg, 2004; Lu & Hof, 2026), von Karman swirling flows (Burghelea *et al.*, 2007), and planar channel-flows (Pan *et al.*, 2013; Qin & Arratia, 2017). However, experiments cannot fully resolve the spatiotemporal structure of the polymer stresses that drive the dynamics. This makes direct numerical simulations (DNS) a necessary and complementary tool: they offer complete access to the fields of interest, such as the velocity and the polymeric stresses, and enable controlled variation of physical parameters, such as elasticity and concentration.

Previously, purely elastic turbulence in pressure-driven channel flows was shown to be organised around coherent structures localised near the channel centreplane. In two dimensions, these structures take the form of travelling-wave states which arise from the centre-mode instability and persist subcritically into the low-Re regime (Berti *et al.*, 2008; Berti & Boffetta, 2010; Garg *et al.*, 2018; Chaudhary *et al.*, 2019, 2021; Khalid *et al.*, 2021; Page *et al.*, 2020; Morozov, 2022). In three-dimensional channel flows, spatially-localised stress states have been reported and interpreted as being organised around the corresponding two-dimensional solutions (Lellep *et al.*, 2023, 2024). Moreover, Lellep *et al.* (2024) showed that the spatio-temporal dynamics can take two distinct forms: a single isolated structure travelling along the streamwise direction, and a space-filling configuration in which multiple structures tend to cover the centre-plane. Transitions between these two states were also observed. These findings motivate a comparison of the two regimes in terms of both mean observables and statistical properties.

In this work, we consider three-dimensional channel flows and revisit the dynamics reported in Lellep *et al.* (2024). We compare the single-structure and space-filling regimes, observing that the former is associated with higher kinetic energy than the latter. To determine whether the existence of these two distinct nonlinear states depends on the chosen pa-

rameter regime, we analyse a new DNS dataset that comprises more dilute and more elastic polymer solutions. We find that all simulations result in the formation of clearly defined time-dependent single-structure state, even if initialised from space-filling configurations. Finally, we focus on single-structure states and compare the statistics of the elastic stresses driving the flow at two different points in parameter space.

EQUATIONS OF MOTION

We consider a model polymer fluid confined within a straight, three-dimensional channel formed by the gap between two parallel, infinite plates. To drive the flow, a constant external pressure gradient is imposed along the streamwise direction. The fluid motion is described by the simplified Phan-Thien Tanner (sPTT) constitutive model (Phan-Thien & Tanner, 1977) coupled with the Navier-Stokes equation:

$$\partial_t \boldsymbol{c} + \boldsymbol{u}\cdot\nabla\boldsymbol{c} - (\nabla\boldsymbol{u})^T\cdot\boldsymbol{c} - \boldsymbol{c}\cdot(\nabla\boldsymbol{u}) = \kappa\nabla^2\boldsymbol{c} - \frac{\boldsymbol{c}-\mathbb{I}}{\mathrm{Wi}}\left[1-3\varepsilon+\varepsilon\,\mathrm{Tr}\,\boldsymbol{c}\right], \quad (1)$$

$$\partial_t \boldsymbol{u} + \boldsymbol{u}\cdot\nabla\boldsymbol{u} = -\nabla p + \frac{\beta}{\mathrm{Re}}\nabla^2\boldsymbol{u} + \frac{1-\beta}{\mathrm{Re\,Wi}}\nabla\cdot\boldsymbol{c} + \frac{2}{\mathrm{Re}}\hat{\mathbf{x}}, \quad (2)$$

$$\nabla\cdot\boldsymbol{u} = 0, \quad (3)$$

where $\boldsymbol{c}$ is the polymer conformation tensor, $\boldsymbol{u}$ is the velocity field, and p is the pressure. Moreover, ε is the shear-thinning parameter, κ is the polymeric stress diffusivity, and $\beta = \eta_s/(\eta_s+\eta_p)$ is the relative contribution of the solvent viscosity η_s to the total fluid viscosity, where η_p is the polymer contribution to the viscosity. Note that β can be seen as a proxy for the polymer concentration, with larger values of β corresponding to a more dilute polymer solution. Finally, the flow is controlled by the Reynolds, Re, and Weissenberg, Wi, numbers, where the latter is defined as the ratio between the typical laminar shear rate and the polymer relaxation time; see (Lellep *et al.*, 2024) for further details.

The computational domain is selected to be periodic along the streamwise and spanwise directions, denoted here by the x and z Cartesian coordinates, respectively, and confined between solid boundaries in the wall-normal direction, y. The lengths of the domain are selected to be $L_x = L_z = 10$ and $L_y = 2$, measured in units of the channel halfwidth. At the walls, we impose no-slip boundary conditions for the velocity, i.e. $\boldsymbol{u}(x, y=\pm1, z, t) = 0$, while the boundary conditions for the conformation tensor are obtained by imposing that $\boldsymbol{c}$ at the walls is equal to the corresponding value obtained by solving the constitutive model Eq. (1) with $\kappa = 0$ (Thomas *et al.*, 2006). The equations of motion, Eqs. (1)-(3), are stepped forward in time using an MPI-parallel fully-dealiased pseudo-spectral code developed within the Dedalus framework (Burns *et al.*, 2020). Time-discretisation is performed using a 4th-order semi-implicit BDF scheme (Wang & Ruuth, 2008) with the timestep dt.

In this work we focus on two datasets, A150 and B150, as shown in Table 1. Both datasets employ $\beta = 0.8$, $\varepsilon = 10^{-3}$, $\kappa = 5.0\times10^{-5}$, $\mathrm{Re} = 0.01$, and $\mathrm{Wi} = 150$. The dataset B150 corresponds to the $\mathrm{Wi} = 150$ simulation reported in Lellep *et al.* (2024), while A150 represents a more dilute and more elastic polymer solution. Simulations are performed with $dt = 2.5\times10^{-3}$ for A150 and $dt = 5.0\times10^{-3}$ for B150 datasets. The spatial resolution is set by (N_x, N_y, N_z) - the number of Fourier, Chebyshev, and Fourier modes used to represent dynamical fields along the corresponding directions; here, we use $(N_x, N_y, N_z) = (512, 128, 256)$ and $(N_x, N_y, N_z) = (256, 1024, 256)$ for A150 and B150, respectively.

id	M_{dof}	$1 - E/E_{lam}$	β	ε
A150	$1.7\cdot10^8$	0.036	0.9	5×10^{-5}
B150	$6.8\cdot10^8$	0.012	0.8	10^{-3}

Table 1. Dataset parameters. Here, $M_{dof} = 10N_x\times N_y\times N_z$ is the total number of the degrees of freedom in each simulation corresponding to spatial representation of the three velocity components, six components of the polymer conformation tensor, and the pressure. The mean values of the kinetic energy and its laminar value are respectively E and E_{lam}.

SPATIOTEMPORAL PATTERNS

In Fig. 1, we present typical kinetic energy timeseries indicating the presence of chaotic dynamics. In the absence of inertia, these dynamics are driven by repetitive cycles of polymer stretching in the presence of local velocity gradients, advection of the stretched polymers by the local velocity field, and polymer relaxation that regenerates velocity gradients at a different spatial location. In Fig. 1, we demonstrate the spatial nature of this process by visualising the local polymer stretch for several instanteneous configurations, indicated by markers.

In the bottom panels of Fig. 1, the first two snapshots correspond to a space-filling state, with the interval between them being clearly stationary with respect to the kinetic energy. Between the second and third snapshots, the dynamics slowly approach a single-structure state, with breakup and merging events of two or more structures occurring within this interval (not shown). The single-structure regime, shown in the third panel, is associated with comparatively weak fluctuations over the interval $90 \lesssim t/\mathrm{Wi} \lesssim 108$. Subsequently, a sharp decrease in the kinetic energy, i.e. a larger $y-$axis value in Fig. 1, signals the return of a space-filling state, shown on the last panel. More generally, space-filling states are less energetic than single-structure states because they are associated with larger polymer stresses, leading to an enhanced drain of kinetic energy in favour of polymeric activity. This is quantified below.

A completely different scenario occurs in the run of dataset A150 which presents a lower value of polymers concentration and a larger elasticity due to less shear thinning. In this case, the spatio-temporal pattern is only constituted by a single-structure moving along the channel centre-plane. A representative configuration can be observed in Fig. 2 where the polymeric stresses, identified by $\mathrm{Tr}\,\boldsymbol{c}$, are visualised. Such visualisation appears more elongated than the third bottom-panel of Fig. 1 being clearly a consequence of the larger elasticity of the former configuration. It is worth noting that dataset A150 originates from a space-filling state obtained in elasto-inertial turbulence simulations at $\mathrm{Re} \gg 1$, from which the control parameters were changed. The subsequent transition to a single-structure state is presented and discussed in Capocci *et al.* (2026*b*), and was later extended up to 260 relaxation times in the simulations of Capocci *et al.* (2026*a*); throughout this evolution, only single-structure states were observed. We

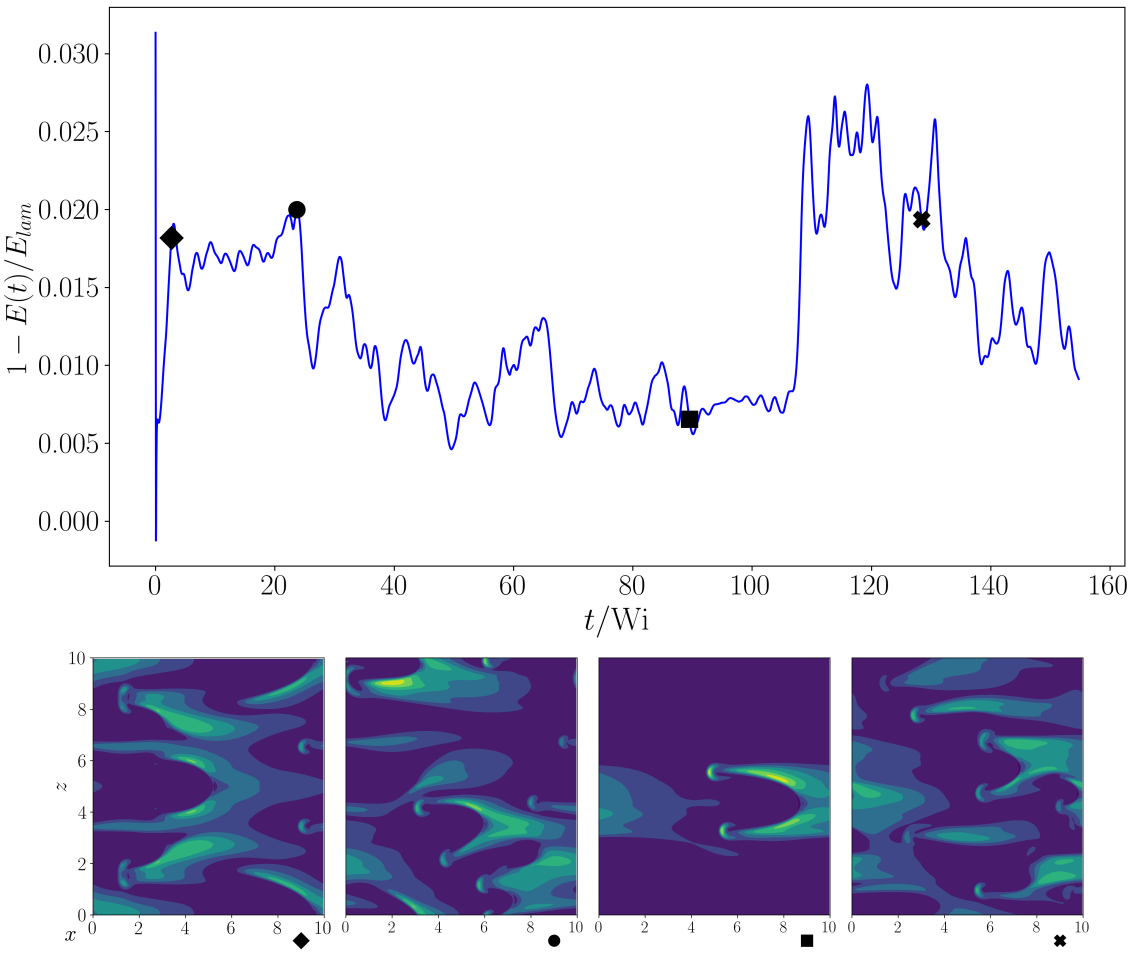

Figure 1. Kinetic energy evolution and polymeric stresses visualisations for dataset B150. Top panel: time series of the mean kinetic energy normalised by the kinetic energy of the laminar state. Bottom panels: centre-plane visualisations of $\mathrm{Tr}\boldsymbol{c}$ where the colour-map values are normalised by $\max(\mathrm{Tr}\boldsymbol{c})$. The symbols indicate instances in time corresponding to the polymeric stress visualisations.

also note that the space-filling to single-structure transition of dataset A150 was tested with different computational domain resolution (not shown). Specifically, the individual number of spectral mode along the domain directions N_x, N_y and N_z was altered resulting in an equal, smaller or higher values of number of degrees of freedoms M_{dof}. In all of these changes we observed a clear transition into a single structure state. This potentially indicates that the space-filling state is specific to the chosen parameter values, particularly β and ε, or, potentially, even to the computational domain length L_x and L_z.

POLYMERIC STRESSES STATISTICS

To further quantify the differences between the space-filling and single-structure regimes, we examine the statistics of the polymer stretch at the channel midplane. As discussed above, polymer stretching, and hence the elastic energy stored by the polymers, can be associated with the trace of the conformation tensor, $\mathrm{Tr}\boldsymbol{c}$. This association can be formalised within the kinetic theory of diluted polymer solutions (Bird *et al.*, 1987; Larson, 1999; Morozov & Spagnolie, 2015), according to which $\boldsymbol{c}$ is identified with the ensemble-averaged tensor product $\langle \boldsymbol{RR} \rangle$, where $\boldsymbol{R}$ denotes the end-to-end vector of a linear polymer molecule. The conformation tensor is normalised such that, in the absence of flow, $\boldsymbol{c} = \boldsymbol{I}$, where $\boldsymbol{I}$ is the identity matrix. Hence, this motivates the study of the statistics of

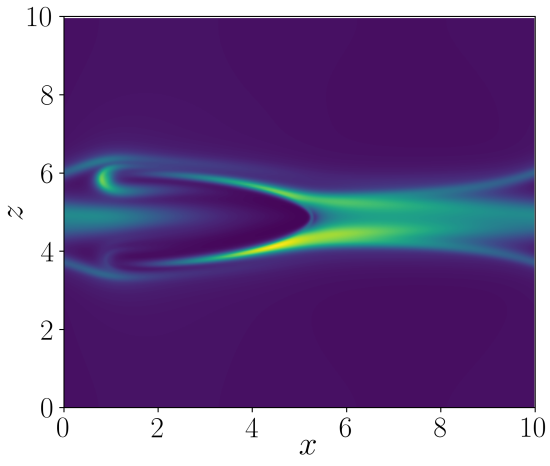

Figure 2. Centre-plane visualisation of $\mathrm{Tr}\boldsymbol{c}$ for dataset A150. The colour-map values are normalised by $\max(\mathrm{Tr}\boldsymbol{c})$.

$\mathrm{Tr}\boldsymbol{c}$ as a natural way to discriminate between single-structure and space-filling states providing information about the typical level of polymer stretching.

Figure 3 shows the PDFs of $\mathrm{Tr}\boldsymbol{c} - 3$, where the equilibrium value has been subtracted. The most immediate ob-

servation is that dataset A150 exhibits substantially broader fluctuations than both the cases belonging to B150; this is remarkable as the two datasets share several physical parameters like Wi. This difference is consistent with the smaller shear-thinning parameter in A150, which permits stronger polymer stretching. A second notable difference appears in the low-stress region of the PDFs. In the space-filling states of dataset B150, the peak at small stresses is strongly suppressed. This behaviour reflects the underlying spatial organisation of the flow. When the midplane is populated by many interacting structures, only a small fraction of the domain remains close to equilibrium. By contrast, in the single-structure regime, the localised high-stress region is embedded within a much larger area where the polymer conformation stays close to its equilibrium value. Consequently, low-stress events are far more prominent in the single-structure PDFs, of both datasets A150 and B150. Finally, still in the single-structure regime, the PDFs retains a tail extending down to probability density values of order 10^{-7}. This indicates that, although the dynamics is organised around a large-scale coherent structure, it still sustain rare and intense stretching events. Conversely, the suppression of the low-stress peak in the space-filling state necessarily results in a larger mean value comapred to the single-structure counterpart. This is consistent with the discussion above where the lower kinetic energy of the space-filling state was associated with stronger polymeric activity which can be roughly interpreted as a larger amount of elastic energy stored in the flow.

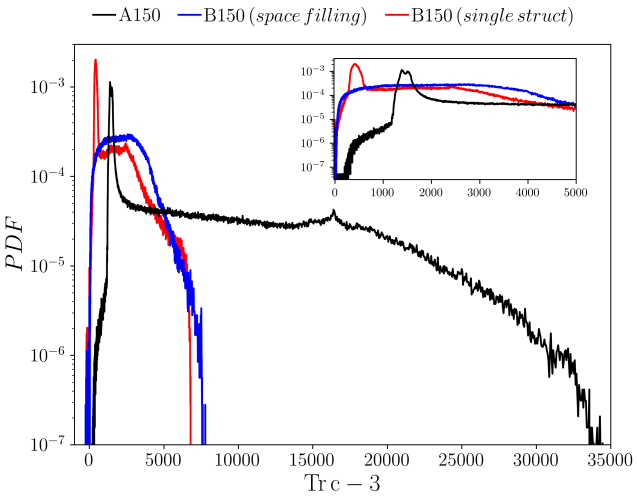

Figure 3. PDF of Tr$\boldsymbol{c}$ at the channel centre-plane belonging to datasets A150 and B150, where in the latter single-structure and space-filling states are discriminated. The inset is a magnification of the x-axis region $[0, 3000]$.

CONCLUSIONS

The first three-dimensional numerical study of purely elastic turbulence in pressure-driven channel flow showed that the dynamics of such flows are organised around structures localised near the channel midplane. The emerging spatio-temporal pattern can take the form of either a single isolated structure or a space-filling state extending across the centre-plane. After expanding the parameter space by considering a more diluted solution of more elastic polymers, however, we observe only single-structure states, even when the simulations are restarted from space-filling configurations. More generally, the space-filling state is associated with a lower kinetic energy than the single-structure state, consistent with stronger polymer-stress activity and a more efficient transfer of kinetic energy into elastic stresses. This distinction is also reflected in the statistics of the polymeric stresses, which show clear differences between the two flow types. Taken together, these results suggest that space-filling dynamics are not universal, but depend sensitively on the viscoelastic parameter regime, whereas the organisation of the flow around midplane-localised structures appears to be a robust feature of purely elastic turbulence in straight channels.

ACKNOWLEDGMENTS

This work used the ARCHER2 UK National Supercomputing Service (https://www.archer2.ac.uk) (Beckett *et al.*, 2024). Support from the UK Turbulence Consortium (EPSRC grant EP/X035484/1) and ARCHER2 team are gratefully acknowledged.

REFERENCES

Beckett, G., Beech-Brandt, J., Leach, K., Payne, Z., Simpson, A., Smith, L., Turner, A. & Whiting, A. 2024 Archer2 service description. Zenodo. https://doi.org/10.5281/zenodo.14507040.

Berti, S., Bistagnino, A., Boffetta, G., Celani, A. & Musacchio, S. 2008 Two-dimensional elastic turbulence. *Phys. Rev. E* **77**, 055306.

Berti, S. & Boffetta, G. 2010 Elastic waves and transition to elastic turbulence in a two-dimensional viscoelastic kolmogorov flow. *Phys. Rev. E* **82**, 036314.

Bird, R. B. 1987 *Dynamics of Polymeric Liquids: Fluid Mechanics*, 2nd edn., , vol. 1. New York: Wiley.

Bird, R. B., Curtiss, C. F., Armstrong, R. C. & Hassager, O. 1987 *Dynamics of polymeric liquids*, 2nd edn., , vol. 2. Kinetic theory. New York: Wiley.

Burghelea, Teodor, Segre, Enrico & Steinberg, Victor 2007 Elastic turbulence in von karman swirling flow between two disks. *Phys. Fluids* **19** (5), 053104.

Burns, Keaton J., Vasil, Geoffrey M., Oishi, Jeffrey S., Lecoanet, Daniel & Brown, Benjamin P. 2020 Dedalus: A flexible framework for numerical simulations with spectral methods. *Phys. Rev. Res.* **2**, 023068.

Capocci, Damiano L, Linkmann, Moritz & Morozov, Alexander 2026*a* (in preparation) .

Capocci, Damiano L, Linkmann, Moritz & Morozov, Alexander 2026*b* Taming the loss of positive-definiteness in direct numerical simulations of elastic turbulence, (in preparation) .

Chaudhary, Indresh, Garg, Piyush, Shankar, V & Subramanian, Ganesh 2019 Elasto-inertial wall mode instabilities in viscoelastic plane poiseuille flow. *J. Fluid Mech.* **881**, 119–163.

Chaudhary, Indresh, Garg, Piyush, Subramanian, Ganesh & Shankar, V. 2021 Linear instability of viscoelastic pipe flow. *J. Fluid Mech.* **908**, A11.

Garg, Piyush, Chaudhary, Indresh, Khalid, Mohammad, Shankar, V. & Subramanian, Ganesh 2018 Viscoelastic pipe flow is linearly unstable. *Phys. Rev. Lett.* **121**, 024502.

Groisman, Alexander & Steinberg, Victor 2000 Elastic turbulence in a polymer solution flow. *Nature* **405** (6782), 53–55.

Groisman, Alexander & Steinberg, Victor 2004 Elastic turbulence in curvilinear flows of polymer solutions. *New J. Phys.* **6**, 29.

Khalid, Mohammad, Shankar, V. & Subramanian, Ganesh 2021 Continuous pathway between the elasto-inertial and elastic turbulent states in viscoelastic channel flow. *Phys. Rev. Lett.* **127**, 134502.

Larson, R. G. 1999 *The structure and rheology of complex fluids*. Oxford University Press.

Lellep, Martin, Linkmann, Moritz & Morozov, Alexander 2023 Linear stability analysis of purely elastic travelling-wave solutions in pressure-driven channel flows. *J. Fluid Mech.* **959**, R1.

Lellep, Martin, Linkmann, Moritz & Morozov, Alexander 2024 Purely elastic turbulence in pressure-driven channel flows. *Proc. Natl. Acad. Sci. U.S.A.* **121** (9), e2318851121.

Lu, Ziyin & Hof, Björn 2026 Multiple states of turbulence at vanishing inertia. *arXiv preprint arXiv:2602.23498* .

Morozov, Alexander 2022 Coherent structures in plane channel flow of dilute polymer solutions with vanishing inertia. *Phys. Rev. Lett.* **129**, 017801.

Morozov, Alexander, Lellep, Martin, Capocci, Damiano & Linkmann, Moritz 2025 Narwhals and their blessings: exact coherent structures of elastic turbulence in channel flows.

Morozov, Alexander & Spagnolie, Saverio E 2015 Introduction to complex fluids. In *Complex fluids in biological systems*, pp. 3–52. Springer.

Page, Jacob, Dubief, Yves & Kerswell, Rich R. 2020 Exact traveling wave solutions in viscoelastic channel flow. *Phys. Rev. Lett.* **125**, 154501.

Pan, L., Morozov, A., Wagner, C. & Arratia, P. E. 2013 Nonlinear elastic instability in channel flows at low Reynolds numbers. *Phys. Rev. Lett.* **110**, 174502.

Phan-Thien, Nhan & Tanner, Roger I. 1977 A new constitutive equation derived from network theory. *J. Non-Newtonian Fluid Mech.* **2**, 353–365.

Qin, Boyand & Arratia, Paulo E.. 2017 Characterizing elastic turbulence in channel flows at low Reynolds number. *Phys. Rev. Fluids* **2**, 083302.

Thomas, D.G., Al-Mubaiyedh, U.A., Sureshkumar, R. & Khomami, B. 2006 Time-dependent simulations of non-axisymmetric patterns in Taylor–Couette flow of dilute polymer solutions. *J. Non-Newton. Fluid Mech.* **138**, 111–133.

Wang, Dong & Ruuth, Steven J 2008 Variable step-size implicit-explicit linear multistep methods for time-dependent partial differential equations. *J. Comput. Math.* **26**, 838–855.